Fabrication of Surface Energy/Chemical Gradients Using Self-Assembled Monolayer Surfaces

S. Meyyappan, M. R. Shadnam, and A. Amirfazli*

Department of Mechanical Engineering, University of Alberta, Edmonton, Alberta, T6G 2G8 Canada

Direct laser patterning of surface energy gradients for alkanethiols on gold has been demonstrated. A homogeneous 1-hexadecanethiol self-assembled monolayer (SAM) on gold (supported by a glass substrate) was selectively desorbed using a focused laser beam. By continually varying the incident laser intensity along a straight line scan, a gradient in desorption was produced. This desorption gradient was then backfilled with the second SAM (16-mercaptohexadecanoic acid), to produce a wettability gradient. The gradient in wettability was characterized by condensation imaging. Secondary ion mass spectroscopy was also used to show variation of the second SAM population from maximum to zero along the length, representative of the chemical gradient. The hexadecanethiol desorption was found to be the most sensitive in a laser intensity range of 29.15–6.5 kW/cm^2. By considering the functional behavior of the governing equations, the theoretical trend for desorption as a function of laser intensity (represented by the out-of-focus distance) was determined. It was found to conform to the experimental data. The proposed method is fast, simple, noncontact, and flexible in terms of producing different types of gradients.

1. Introduction

A surface having a gradual variation in surface energy/property in the nano-, micro-, or millimeter scale is termed as a surface with an energy gradient. Surface energy gradient based self-propulsion of liquids has been of interest to researchers for directing drop movements.[1,2] Surface energy gradients are also of interest for biological applications such as cell migration[3] and protein adsorption studies.[4] The main objective of this paper was to demonstrate a novel method to fabricate surface energy gradient features using self-assembled monolayers (SAM) of thiol on gold.

A SAM is a thin organic film on a substrate, formed by spontaneous adsorption of molecules from the corresponding solutions. SAM surfaces exhibit properties as a function of the tail group of the adsorbed molecules. A typical example is alkanethiol SAM (HS(CH$_2$)$_n$X), where X can be CH$_3$, COOH, or NH$_2$, etc. on gold. The SAMs are of widespread interest when surface properties/energy needs to be manipulated. For example, by replacing the homogeneous alkanethiol SAM molecules having a CH$_3$ tail group (hydrophobic) with SAM molecules having a different tail group COOH (hydrophilic), the surface properties/energy can be manipulated. If the replacement of the second SAM molecule is as shown in Figure 1c, then the resulting surface would exhibit a gradient in surface energy/property.

Surface energy gradients using SAMs have been produced as early as 1987 by Elwing et al.[5] In the earliest method and subsequent refinements,[6-9] the gradients were produced by molecular diffusion of chlorosilanes in a gas/liquid phase on a
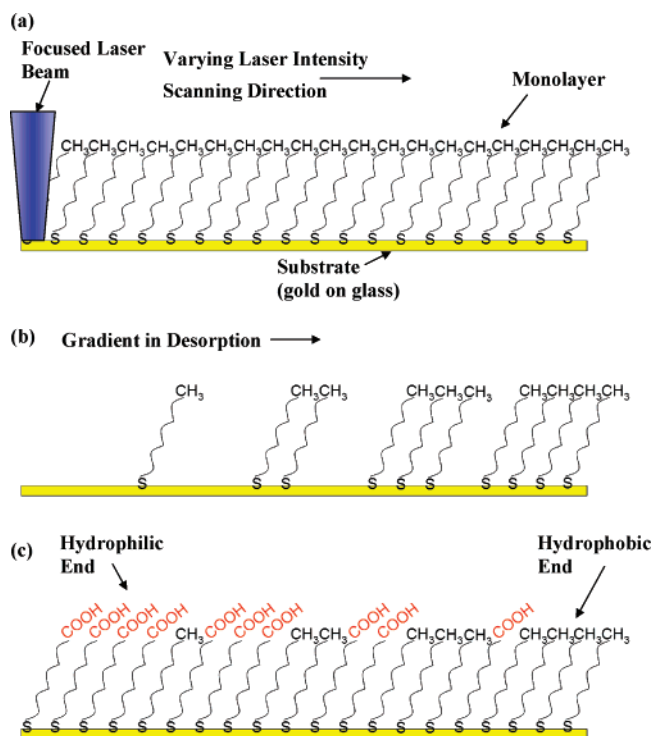

Figure 1. Three steps in the production of surface energy gradients using DLP. (a) Focused laser beam on homogeneous hydrophobic hexadecanthiol SAM, (b) laser intensity is varied along the scan direction to produce a gradient in desorption, (c) backfilling of the desorption gradient with mercaptohexadecanoic acid (the second SAM). The population of the second SAM molecule (COOH tail group) changes from a maximum at the hydrophilic end to zero at the hydrophobic end, creating a gradient in surface wetting.

silicon or silicon dioxide substrate. The diffusion of the chlorosilane molecules (hydrophobic) on silicon or silicon dioxide

* Corresponding author. Tel.: (780) 492-6711; fax: (780) 492-2200; e-mail: a.amirfazli@ualberta.ca.

(1) Chaudhury, M. K.; Whitesides, G. M. *Science (Washington, DC, U.S.)* **1992**, *256*, 1539.

(2) Zorba, V.; Persano, L.; Pisignano, D.; Athanassiou, A.; Stratakis, E.; Cingolani, R.; Tzanetakis, P.; Fotakis, C. *Nanotechnology* **2006**, *17*, 3234–3238.

(3) Gunawan, R. C.; Silvestre, J.; Gaskins, H. R.; Kenis, P. J. A.; Leckband, D. E. *Langmuir* **2006**, *22*, 4250–4258.

(4) Sethuraman, A.; Han, M.; Kane, R. S.; Belfort, G. *Langmuir* **2004**, *20*, 7779–7788.

(5) Elwing, H.; Welin, S.; Askendal, A.; Nilsson, U.; Lundstrom, I. *J. Colloid Interface Sci.* **1987**, *119*, 203–210.

(6) Elwing, H.; Askendal, A.; Lundstrom, I. *J. Biomed. Mater. Res.* **1987**, *21*, 1023–1028.

(7) Elwing, H.; Welin, S.; Askendahl, A.; Lundstrom, I. *J. Colloid Interface Sci.* **1988**, *123*, 306–308.

(8) Elwing, H.; Askendal, A.; Lundstrom, I. *J. Colloid Interface Sci.* **1989**, *128*, 296–300.

(9) Elwing, H.; Goelander, C. *Adv. Colloid Interface Sci.* **1990**, *32*, 317.

(hydrophilic) was controlled such that the resulting surface had a gradient in wettability. Although surface energy gradients having continuously changing wetting (120−10° water contact angle) were produced using molecular diffusion based methods, gradients of different shapes were not possible, and the length of the gradient was restricted by the maximum distance over which diffusion could occur. Furthermore, there was little control over the surface energy variation rate or steepness of the gradient. Also, since the gradient was produced by the controlled diffusion of the hydrophobic chlorosilane molecules on the hydrophilic substrate, the surfaces exhibited a gradient in wetting alone. As such, there were restrictions on the types of gradients produced (i.e., different types of gradients such as gradients in surface charge, polarity, or biocompatibility were not possible). However, in 1995, Liedberg and Tengvall[10] reported a method based on cross-diffusion of molecules. In this technique, different alkanethiol SAM molecules were cross-diffused from opposite ends of a polysaccharide matrix placed on gold. Although this method has the flexibility of using different chemical combinations (using two SAM species) to produce different types of gradients, the other issues discussed previously remained largely unaddressed.

Gradients have also been produced by the oxidation of silanes.[11] The alkylchlorosilane monolayer (hydrophobic) chemisorbed on silicon (hydrophilic) was selectively oxidized and removed to produce wettability gradients. The graded oxidation of the silane monolayer was achieved by UV exposure through variable density filters.[11] Techniques based on oxidation have also been used to produce gradients on polymeric substrates.[12,13] The variation in the degree of oxidation was achieved either by a scanning radio frequency (RF) discharge[12] or a scanning corona RF discharge.[13] Two very recent methods are (1) photodegradation of the alkylsilane monolayer, in which the octadecyltrimethoxysilane monolayer (hydrophobic) was photodegraded under vacuum with ultraviolet radiation at 172 nm through mesh filters to produce wettability gradients[14] and (2) a photocatalytic lithography method,[15] in which a thiol monolayer on gold was exposed to a UV light that passed through a graded photomask and a TiO$_2$ covered glass (the thin TiO$_2$ film acted as a catalyst to oxidize the thiol). Using these techniques based on oxidation and photodegradation, in combination with different masks, gradients of different shapes and lengths could be produced. However, all such methods directly or indirectly need to use photolithography, which requires expensive infrastructure, and once the mask is produced, it is difficult to make changes; some also require long processing times on the order of 1 h.[15] These factors make such methods cumbersome, inflexible, and/or expensive. A technique capable of producing gradients of different types, using two or more SAM species, and that is also flexible to produce gradients of different shape, length, and steepness is required.

In this study, we developed a novel technique based on direct laser patterning (DLP),[16,17] to produce surface energy gradient features. The proposed method can be used to produce different types of gradients using contrasting SAM molecules (even more

than two species). Further, the method has capabilities to produce gradients of different shapes, lengths, steepnesses, and widths, without the need of photolithography either directly or indirectly. The application of DLP to produce gradients is shown in Figure 1: it is a three-step process similar to the scanning tunneling microscopy (STM) replacement method of Fuierer et al.,[18] but it is much faster and complimentary to the nanometer-sized gradients produced in the STM method (i.e., it can produce gradients of the order of a micro- to centimeter in scale). The steps are as follows: formation of a homogeneous SAM on a substrate by solution deposition, followed by the selective desorption of the SAM molecules on the substrate using a laser beam. DLP works by thermally desorbing the SAM, which is controlled by laser intensity.[16,17] In the proposed method to produce surface energy gradients using DLP, the laser intensity is continuously varied along the scan path to produce a gradient in desorption as shown in Figure 1b. This desorption gradient is then backfilled with the second SAM molecule (with a different tail group) in the final step to produce a line pattern having a gradient in the surface energy/property (see Figure 1c). In principle, this method can be repeated more than once to produce multi-species surfaces. The feasibility of the proposed method is demonstrated by producing wettability gradient features using hexadecanethiol (HDT) and mercaptohexadecanoic acid (MHA) as the contrasting SAMs. The method can also be used for producing gradients using an alkylsilane monolayer on silicon, by modifying the DLP technique used in ref 19.

2. Materials and Methods

2.1. Sample Preparation. The samples were made using 1 mm thick premium microscopic slides (Fisher Scientific Co.) as the substrate. A 50 Å titanium adhesion layer was sputtered on the microscopic slides at a rate of 0.30 Å/s followed by a 300 Å gold layer at a rate of 0.98 Å/s on top of it. After completion of sputtering with gold, the sample was immersed in a 1 mM ethanolic solution of HDT (Fluka) for 48 h to form the primary SAM.

2.2. Experimental Setup. The schematic of the setup used is shown in Figure 2. A continuous wave (CW) argon ion laser (Melles Griot 543-BS-A03) at 488 nm was used as the laser source. The half wave plate combined with the Glan polarizer was used to control the laser power through the optical train. The wedge in the optical setup was used to sample the beam (∼4%) for online power measurement. The quarter wave plate was used to avert the destructive interference of the incident and reflected laser beam (from the sample). The mirrors were used for steering the laser onto the sample. The apertures were used for aligning the laser beam before patterning. An automated beam blocker was employed for the purpose of blocking the laser beam temporarily (i.e., when patterning needed to be paused or there was a need to have a break in the pattern design). The microscopic objective (10×) used for focusing the laser beam was mounted on a micrometer driven translational stage. The sample holder was attached to a tilt stage on a computer controlled two-axis translational stage. The focal distance of the objective was determined by forming an image of the sample in the CCD camera using a white light source, as shown in Figure 2. The focal distance obtained needed to be corrected by an offset to obtain the focal distance for the laser beam due to the difference in wavelength of the laser and the light source used. This correction factor was determined to be +131 μm for this setup as configured (note that the objective used has multiple proprietary lenses packed within the 10× casing; hence, the correction factor needed to be determined experimentally).

(10) Liedberg, B.; Tengvall, P. *Langmuir* **1995**, *11*, 3821.

(11) Roberson, S. V.; Fahey, A. J.; Sehgal, A.; Karim, A. *Appl. Surf. Sci.* **2002**, *200*, 150−164.

(12) Pitt, W. G. *J. Colloid Interface Sci.* **1989**, *133*, 223−227.

(13) Lee, J. H.; Kim, H. G.; Khang, G. S.; Lee, H. B.; Jhon, M. S. *J. Colloid Interface Sci.* **1992**, *151*, 563−570.

(14) Ito, Y; Heydari, M.; Hashimoto, A.; Konno, T.; Hirasawa, A.; Hori, S.; Kurita, K.; Nakajima, A. *Langmuir* **2007**, *23*, 1845−1850.

(15) Blondiaux, N.; Zurcher, S.; Liley, M.; Spencer, N. D. *Langmuir* **2007**, *23*, 3489−3494.

(16) Shadnam, M. R.; Kirkwood, S. E.; Fedosejevs, R.; Amirfazli, A. *Langmuir* **2004**, *20*, 2667−2676.

(17) Shadnam, M. R.; Kirkwood, S. E.; Fedosejevs, R.; Amirfazli, A. *J. Phys. Chem. B* **2005**, *109*, 11996−12002.

(18) Fuierer, R. R.; Carroll, R. L.; Feldheim, D. L.; Gorman, C. B. *Adv. Mater.* **2002**, *14*, 154−157.

(19) Hartmann, N.; Balgar, T.; Bautista, R.; Franzka, S. *Surf. Sci.* **2006**, *600*, 4034−4038.

(20) Kumar, A.; Whitesides, G. M. *Science (Washington, DC, U.S.)* **1994**, *263*, 60−62.
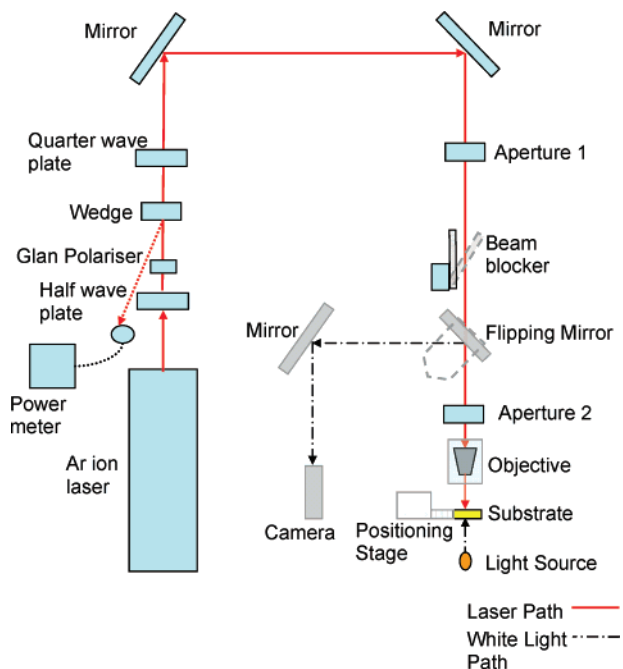
Figure 2. Schematic of the experimental setup for the fabrication of surface energy gradients using DLP for self-assembled monolayers. Apertures 1 and 2 are shown and were used for fine and coarse alignment of the laser beam, respectively. The light source shown was used for determining the focal distance of the objective (note that with a 300 Å gold layer, the samples were semi-transparent).

2.3. Experimental Methodology. To fabricate surface energy gradients using DLP, the incident laser intensity needs to be continually varied along the length of the scan. This is achieved by scanning the sample, which was kept inclined at a suitable angle to the focal plane of the laser beam (see Figure 3). The incident beam spot radius increased from an initial value at the focused end to a larger value at the out-of-focus end, due to the divergence of the laser beam (see Figure 3). Hence, the incident laser intensity varied from a maximum to a minimum. The minimum was determined by the threshold laser intensity for which there was no desorption of the HDT SAM. The resulting gradient in desorption of the primary SAM molecules was then backfilled with the second SAM molecule to produce a gradient in the surface energy/property. This process can be repeated multiple times for various species to be used, but here for simplicity, only a two-species sample is shown.

The laser power used for patterning was carefully selected to be well below the damage (to gold) threshold, by conducting a series of experiments in which the laser power was progressively decreased and the substrate checked for damage under an optical microscope (50×). The damage results were compared with previous results.[16] In the final experiments, a laser with a power of 16.26 mW was focused using a $10\times$ (Olympus UPLAN FI) objective onto the substrate (hydrophobic HDT SAM on gold). The incident laser intensity was 204.7 kW/cm^2, corresponding to a beam radius of 1.59 μm (measured). The sample was kept inclined at an angle of 1°6′ 47″ to the focal plane, so that laser intensity reduced to the desorption threshold, determined to be ~1.9 kW/cm^2 at the end of the line scanned (~8 mm long). The sample was scanned at a constant velocity of 200 μm/s to create the desorption gradient in primary SAM (i.e., HDT). Also, as a baseline, a line was scanned by keeping the substrate perfectly perpendicular to the scanning laser beam. The baseline was used as an internal reference, while characterizing the gradient using secondary ion mass spectroscopy (SIMS) or condensation imaging. The patterned sample was then rinsed with ethanol and dried in a stream of nitrogen before immersion into a 1 mM solution of 16-MHA (Sigma Aldrich) for 2 min to backfill the bare or partially bare gold regions. The second SAM (MHA) having a carboxylic tail was hydrophilic and hence will create a gradient in wettability. The samples processed were stored in a chamber filled with nitrogen
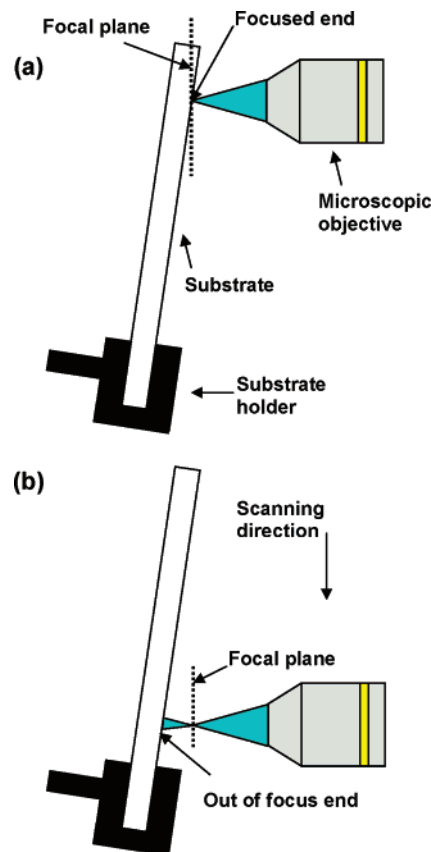

Figure 3. Continuous variation of laser intensity, along the line scan, achieved by keeping the substrate inclined with respect to the focal plane. (a) shows the laser beam focused at a point on the substrate; this point receives the highest laser intensity and hence corresponds to the hydrophilic end of the pattern. The hydrophobic molecules will be fully desorbed and backfilled with a hydrophilic species. (b) shows an out-of-focus laser beam at the other end of the line scan: the laser intensity drops below the threshold for desorption, and hence, this end of the pattern is hydrophobic (no desorption of primary SAM).

until further analysis was conducted. A series of gradient and baselines was produced on a sample and characterized to verify repeatability of the process.

2.4. Characterization. The gradient line features were characterized by secondary ion mass spectroscopy−time-of-flight analysis (SIMS-TOF) to show the gradient in a chemical concentration of the second SAM molecule (MHA) by analyzing the oxygen signal. Also, the gradient in surface energy (wetting) was captured by condensation imaging. SIMS-TOF is an analytical method used to determine the chemical composition in the top few nanometers of a sample. In the particular case of this study, as oxygen is expected to be concentrated along the gradient and baselines (corresponding to the MHA SAM), the sample was bombarded with a 15 keV focused gallium ion beam spot (300 nm) to produce the oxygen distribution image at various locations along the patterns produced on the sample. The mass resolved secondary ion image for oxygen (see Figure 4) with a lateral resolution of 0.78 μm/pixel was formed, by rastering the ion beam over a 200 μm × 200 μm area (256 pixels × 256 pixels) and allotting each pixel a value corresponding to the counts of oxygen ions collected over 100 shots of the ion beam (performed by ion-TOF software). Also, to further investigate the mechanism of patterning, SIMS imaging at a higher lateral resolution (0.34 μm/pixel) was carried out at various positions along the lines using a 25 keV gallium ion beam.

The oxygen ion image at each position was then analyzed using ion-image software. Transverse line scans were procured as shown in Figure 4, to obtain pixel intensity plots along any given point on the patterns imaged (see Figure 5). The distinguishable peaks in the
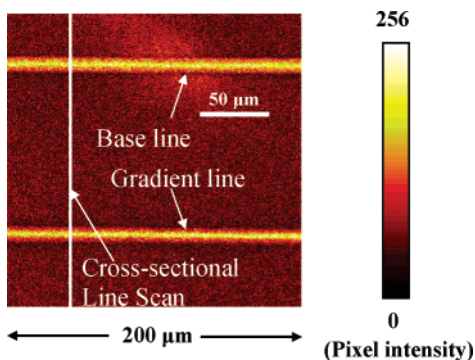
Figure 4. SIMS image for oxygen ion concentration, at the beginning of the base and gradient lines. The lines represented by lighter colors (higher pixel intensities) correspond to higher oxygen concentrations as compared to the background. The image also shows the transverse line scans used to obtain the pixel intensity plot across the line patterns (using the Ion-image software). This procedure was repeated at various locations along the pattern formed.

pixel intensity plots represent the patterned lines. The background (i.e., HDT) in the oxygen ion image is not represented by a single value; it is rather represented by a range of pixel intensities scattered within a range. This is probably due to the noise inherent in this type of instrument due to its channel plate sensitivity differences. Figure 5a−c clearly shows that the pixel intensity peak/oxygen signal for the gradient line decreases from a large value at the beginning (Figure 5a) to a smaller value at the middle (Figure 5b) and fades into the background signal at the end (Figure 5c). To capture the relative quantitative reduction in oxygen concentration, it was required that a characteristic value proportional to the oxygen ions based on the pixel intensity be assigned, as SIMS does not provide absolute quantities of elements. The pixel intensity per unit area was deemed suitable, as it corresponds to the oxygen concentration at the analyzed position in the pattern and can be determined from the pixel intensity plots.

A curve described by two Gaussian components and a constant was fitted (using the Trust-Region algorithm in Matlab) as shown in Figures 5 and 6. The two Gaussian components in Figure 6 determine the fit for the pixel intensity/oxygen concentration peaks; the constant component, fitting a straight line to the scattered pixel intensities, represents the background. A Gaussian shape was selected for the oxygen concentration peaks, as it corresponds to the incident laser beam intensity profile (TEM_{00} mode). The pixel intensity per unit area was determined by calculating the area under the fitted curve (shaded areas under the curves in Figure 6) and dividing it by a circular area corresponding to the thermal footprint of the laser beam (hatched contour areas in Figure 6). The circular area/thermal footprint of the laser beam corresponds to the full pattern width and hence can be calculated based on the Gaussian fit. Hence, the pixel intensity per unit area (pixel intensity concentration) was determined for various positions along the patterns and was used to characterize the gradient in chemical concentration. To take into account the uncertainties associated with the data, five line scans at ∼50 μm intervals were obtained for each position (200 μm × 200 μm), and the corresponding pixel intensity concentrations were calculated. The reported pixel intensity concentration for each position (middle of the scanned area/image) is the average of the values found from five line scans, and the error bars correspond to ±1 SD.

The gradients were also analyzed using condensation imaging, which involved imaging the condensation of water drops on the sample. The samples were cooled using a Peltier cell in an enclosure with an atmosphere of high humidity. Pictures were taken along the length of the gradient line to reveal the gradient in wetting.

3. Results and Discussion

The mechanism of the technique (i.e., the effect of reducing the laser intensity along the scanning direction) needs to be understood before interpreting the results. This is explained in

detail (with reference to the SIMS images) in the following paragraphs. At the initial portion of the scanned line, when the intensity is well above the threshold for desorption, a central region with complete desorption, flanked by very narrow regions of partial desorption that are ultimately delimited by areas where there is no desorption (i.e., background), is observed. The reduction in laser intensity along the scan direction leads to a rapid disappearance of the central full desorption region, leaving only partially desorbed areas. Hence, the lateral gradient present initially (due to a transition from the full desorption to the background) disappears. Longitudinally, the steady decrease in the amount of partial desorption continues until the threshold for desorption is reached, where patterning ceases. Hence, a longitudinal chemical gradient is created along the length of the scanned line.

The mechanism as explained previously was revealed by high-resolution (0.34 μm/pixel) SIMS oxygen ion images. The oxygen ion images (see Figure 7) revealed that the MHA SAM filled the bare or partially bare regions. It can be seen from the leftmost frame in Figure 7 that at the beginning of the laser scan, the patterned base and gradient lines (top and bottom) are represented by a high concentration of oxygen at the center, a lower concentration at the edges, and zero concentration in the background, as mentioned earlier. However, further along the length of the gradient line (see frame 3 in Figure 7), the high oxygen concentration/full desorption region is seen to vanish, leaving only a uniform weaker signal for oxygen, indicating partially desorbed HDT backfilled with MHA. Also, it can be noted that the sharp lateral gradient (in the oxygen concentration/ MHA molecules) present initially, perpendicular to the direction of the scanned line, has vanished. Following this, there is a constant decrease in the oxygen signal for the gradient line, along the length, as can be seen in subsequent frames. This indicates that lesser and lesser MHA has been backfilled (HDT has been desorbed), along the scan, before the oxygen signal finally fades into the background, where there is no patterning. Hence, a longitudinal gradient is created. Further, the baseline is found to be consistent at all the positions along the laser scan.

To verify as to whether the central high oxygen concentration region seen in the SIMS oxygen ion images of the baseline and the gradient line (at the beginning) corresponds to full desorption, a control experiment was performed. A bare gold sample (gold film thickness of 30 nm) was coated with MHA. Subsequently, a SIMS analysis (with parameters the same as high-resolution SIMS images) was performed to obtain the oxygen ion image for fully covered MHA. The average pixel intensity along with the 95% confidence level was found to be 168.5. This was very comparable to the average signal value for the central region seen in Figure 7 (i.e., 163.4). It has been shown that the central high concentration of oxygen in the SIMS image indeed corresponds to the full desorption region but that there is no full desorption region past the initial stages of scanning; in fact, most of the scanned length experiences a partial desorption. The gradient surfaces produced also were characterized by condensation imaging, and the variation of oxygen concentration in the gradient line was quantified by analyzing SIMS images at various positions along the scan direction.

While the substrate was cooled, condensation was first observed to occur on the most hydrophilic regions (the base and gradient lines) of the substrate. This was due to a higher surface energy of the hydrophilic lines as compared to the background. Within a few minutes, condensation was also observed in the primary monolayer/background (a similar behavior was observed previously in ref 21). Apart from differentiating the patterned lines
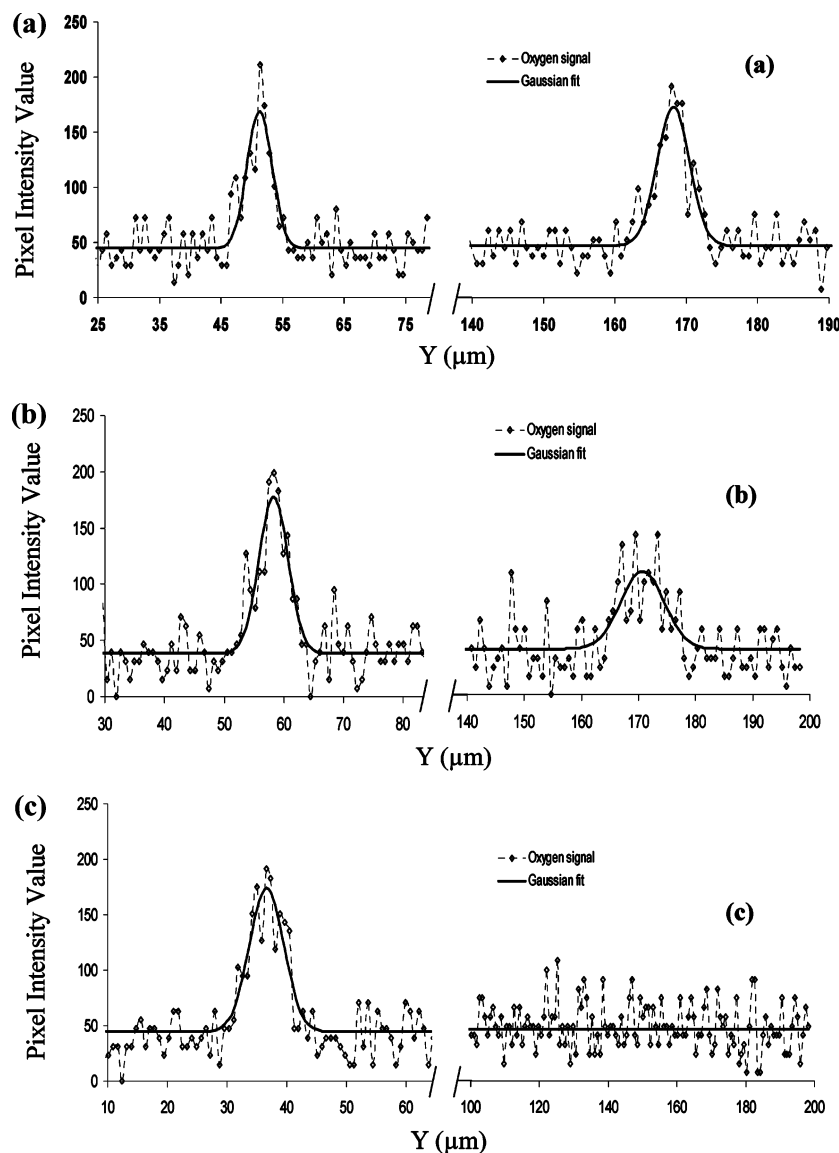
(a)

(b)

(c)

Figure 5. Pixel intensity plot corresponding to the oxygen concentration across the patterns (*y*-axis) along the base and gradient lines. (a) At the beginning, the base and gradient lines have approximately the same oxygen signal. (b) At the middle of the scanned length, the gradient line oxygen signal is lower as compared to the baseline. (c) At the end of the scan, the gradient line oxygen signal has faded into the background signal. At all the positions, the oxygen signal for the baseline remained constant given the experimental uncertainty.

from the background, the condensation patterns also distinguished the base and gradient lines. The differences can be understood by considering the insights, provided by the high-resolution SIMS images. From the SIMS images, it is seen that at the beginning of the scan, there is a sharp lateral gradient. When the surface is cooled, condensation occurs in the full desorption areas and grows due to two reasons: (1) their higher surface energy[21] (as compared to the background) and (2) drops in the partially desorbed areas on either side of the fully desorbed region coalescing with the central ones[22] (due to the lateral gradient). This explains the large drops on the center line and the clearing around it in the baseline (see Figure 8). Further along the scanning direction, when the full desorption area vanishes and only partially desorbed areas are present, there is no sharp lateral gradient and, correspondingly, no clearing in the lateral direction (see Figure 8; note that the image was taken approximately at the three-quarter length of the gradient).

To capture this difference in wetting along the gradient line, condensation images of the base and gradient lines were taken at four positions along the scanned lines as shown in Figure 9. It can be seen that at the beginning of the scan (first picture in Figure 9), the condensed drops on the base and gradient line are consistent in size and shape. Also, it can be noticed that the condensed drops are oval in shape, aligned along the center line, and have a clear surrounding (as explained earlier). At the mid-length of the scan, the drops in the gradient line are found to be smaller and circular as compared to the drops in the baseline (the top line feature in each of the panels). Further, it can be noticed that there is no clearing around the drops in the gradient line, indicative of a relatively homogeneous desorption or no lateral gradient. Finally, in frame 4 in Figure 9, it can be seen that the drops (on the gradient line) merge with the drops in the background, thus revealing that the gradient in surface energy/wettability has ended.

The SIMS oxygen ion images taken at various positions along the length of the gradient and baselines are shown in Figure 10. The patterned lines are shown as brighter areas in the images,

(21) Daniel, S.; Chaudhury, M.; Chen, J. *Science (Washington, DC, U.S.)* **2001**, *291*, 633−636.
(22) Saleh, B. E. A.; Teich, M. C. *Fundamentals of Photonics*; John Wiley and Sons, Inc.: New York, 1991; p 83.
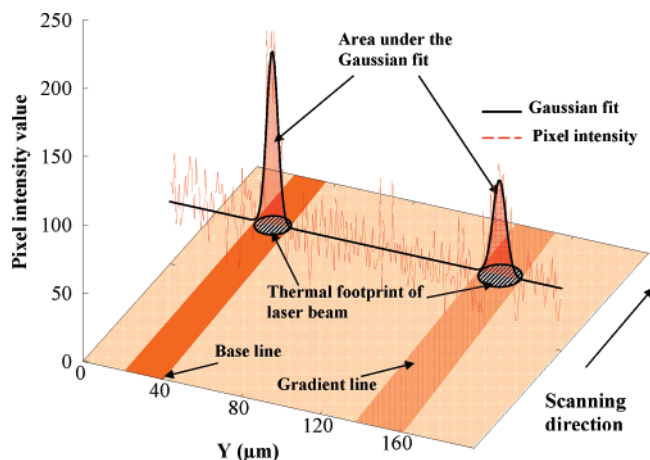
Figure 6. Pixel intensity plot across the patterned lines, a double Gaussian fit (solid heavy line), and the area underneath (hatched area). Hatched areas corresponds to the thermal footprint of the laser beam. The area under the Gaussian fit (shaded) provides the total pixel intensity corresponding to the total counts of oxygen. The total pixel intensity is then divided by a circular area corresponding to the thermal footprint of the laser beam. The diameter of the thermal footprint of the laser beam corresponds to the full width of the pattern and is calculated based on the full width of the Gaussian fit. In comparison to the baseline, it can be seen that the gradient line has a lower value for the oxygen signal and a larger laser footprint, hence a reduced laser intensity due to a diverged incident laser beam.
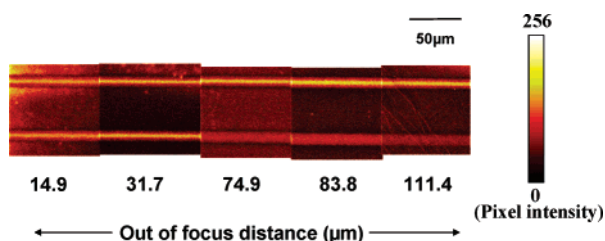

Figure 7. SIMS oxygen ion images from five positions along the laser scan direction. Top line in each frame is the base, and the bottom is the gradient. Laser intensity is reduced from left to right for the gradient line. At the beginning of the scan (see frame 1, leftmost), it can be noted that the gradient and baseline have a high oxygen concentration at the center, less at the edges, and zero in background, representative of complete backfilling of the second SAM at the center, less at the edges, and zero in the background. Further along the scan in frame 3, it can be seen that the central high oxygen concentration area vanishes to leave only a uniform weaker signal for oxygen, representative of backfilling partially bare regions. The signal for oxygen is seen to consistently become weaker along the laser scan direction (in the subsequent frames) before it finally vanishes into the background, representative of a longitudinal chemical gradient.

corresponding to higher oxygen ion counts than the background (HDT). The higher oxygen ion counts in the patterned lines are due to the presence of the second SAM molecules (MHA) having a COOH tail group. It can also be seen from Figure 10 that the gradient line is brighter at the start and gradually fades into the background, which is representative of the reducing oxygen concentration (similar to the condensation imaging). The gradient line totally fades at ~8 mm of the scanned length, at which point the sample is calculated to be ~160 μm out-of-focus. At this point, there is no desorption of the primary SAM (HDT), and the corresponding laser intensity provides the threshold for desorption. On the basis of three replications, it was found that the desorption threshold ranged between 1.79 and 1.95 kW/cm^2. This range was found to agree with the previously determined
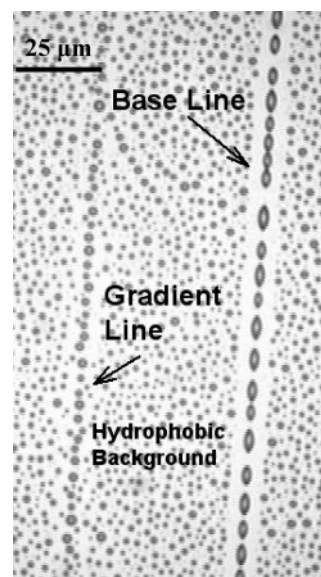

Figure 8. Image of the condensed water drops on the sample at 10× magnification. The image is taken approximately at three-quarters of the scanned length. The widths of both lines are similar. It can be seen that the water droplets wet the gradient and baselines differently. Further, the hydrophobic background corresponding to the hexadecanethiol SAM is seen to be wetted distinctly as compared to the patterned lines.

range of 1.9 and 2.1 kW/cm^2 from ref 16, using a +10 cm lens. Further, it can be seen that the baseline is consistently bright at various positions along the scanned length and hence has a constant oxygen concentration (again similar to the high-resolution SIMS condensation imaging results).

The oxygen ion signal fading into the background along the gradient line signifies the chemical concentration gradient. However, the relative reduction in oxygen concentration (proportional to the relative reduction in the second SAM population) along the length needs to be quantified, so that the trend of surface energy/property variation in the resulting gradient can be found. To quantify the relative reduction in the oxygen concentration, the SIMS images obtained at various positions were processed as mentioned in section 2.4. to determine the pixel intensity per unit area. This quantity, when plotted as a function of the substrate's out-of-focus distance, will allow one to know how to vary the laser intensity to vary the steepness of the gradient. Such a plot generated for the three gradient lines produced is shown in Figure 11. It can be seen that the pixel intensity per unit area proportional to the oxygen concentration decreases with an increasing out-of-focus distance or a decreasing laser intensity. The oxygen concentration is found to be a slowly varying function of the out-of-focus distance up to the point where the sample is 40 μm out-of-focus. The trend is followed by a sharp decrease in the oxygen concentration until the sample is ~90 μm out-of-focus. For out-of-focus values larger than 90 μm, the oxygen concentration was found to be a slowly varying function of the out-of-focus distance before it finally faded into the background (when the sample is ~160 μm out-of-focus). As such, the largest variation in the oxygen concentration takes place when the sample is 40–90 μm out-of-focus. This means that the SAM desorption is the most sensitive to the laser intensity changes, for the range between 29.15 and 6.5 kW/cm^2 and, as such, is useable to produce gradients; this range is named as the partial desorption regime. Also, it can be noted that the pixel intensity concentration varies from a value of 4.8–4.56 to 2.17–2.09 in the partial desorption regime, with limiting values of 5.5–7, when the sample is at the focus of the laser beam (start

Figure 11. Variation of oxygen concentration for three runs of the gradient line, with respect to the out-of-focus of laser beam. Error bars correspond to ± 1 SD. The lines joining the data points are to guide the eye only.

of SAM by laser patterning can be theoretically predicted using a thermokinetic model[17]

$$c(x,y) = c_0(x,y) \exp\left(-\int_{t_0}^{t_1} \frac{K_B T(x,y,t)}{\hbar} \exp\left(-\frac{\Delta G}{RT(x,y,t)}\right) dt\right) \quad (1)$$

where c is the concentration of SAM at a point, c_0 is the initial concentration at a given point, K_B is the Boltzmann constant, $\hbar$ is Planck's constant, ΔG is the Gibbs free energy of activation, R is the universal gas constant, T is temperature, and t is time. It can be seen that temperature is the only variable in the integrand of eq 1. Hence, the integral in the equation is the time integral of the temperature at a particular point. Taking the initial concentration of the HDT SAM (c_0) as 1 (corresponding to a 100% coverage), from eq 1, it can be seen that the SAM concentration after irradiation (c) varies as an exponential function of the negative of the temperature induced. The fraction of HDT desorbed at a point (ψ) can be calculated by subtracting the SAM concentration after irradiation (c) from the initial SAM concentration (c_0) and is given as

$$\psi \propto (1 - \exp(-T)) \quad (2)$$

To be able to plot the variation of the SAM concentration as a function of laser intensity or out-of-focus distance, knowledge of the temperature field is required. The temperature induced by the laser beam can be predicted using the heat diffusion model. From our previous study (i.e., ref 16), the following equation for the temperature rise was implied:

$$T = T_0 + \frac{PA\sqrt{2}}{kr\pi^{3/2}} \int_0^\infty \frac{1}{(U^2 + 1)} \exp \times$$
$$\left\{-2\left(\frac{(X + VU^2)^2 + Y^2}{(U^2 + 1)}\right)\right\} dU \quad (3)$$

where T_0 is room temperature, k is the thermal conductivity of glass, A is the absorptivity of the sample, r is the 2e-folding beam radius, and X, Y, V, and U are dimensionless numbers. They are defined as $X = 2x/r$, $Y = 2y/r$, $V = vr/8D$, and $U = (8Dt/r^2)^{1/2}$, where, v —is the velocity of patterning, D —is the thermal diffusivity, t is time, and x and y are coordinates with x being the scanning direction. It can be seen that the integrand in eq 2 is dimensionless. The term outside the integral has terms such as the power (p), thermal conductivity (k), and absorptivity (A), which are all constants. This quasi-static equation can be used to predict the temperature profile induced at a position. For the case studied, considering the temperature induced at a series

Figure 9. Condensation images of the base and gradient lines at various distances from the start point of the scan (10× magnification). It can be seen at the start point of scan that the gradient and baseline appear to be consistently wetted. The image at ∼4 mm from the starting point shows that the drops in the gradient line have shrunk in size, corresponding to a lower wettability. This trend continues and can be seen in the image at ∼6 mm and finally at ∼8 mm from the start as the gradient line fades into the hydrophobic background.
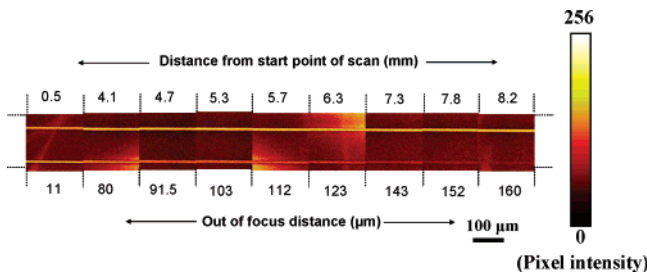

Figure 10. SIMS oxygen ion images of the base (top) and gradient lines (bottom). The images at various distances from the start are juxtaposed to show the relative variation in oxygen concentration. The scale bars shown apply to each of the juxtaposed images. It can be seen that the baseline at the top has a uniform color (pixel value) representative of the consistent oxygen concentration, whereas the gradient line (bottom) consistently fades and merges into the background at the end, thus showing the gradient in chemical concentration.

of gradient) and 1–1.6 when the sample is 145–150 μm out-of-focus (just before the gradient line fades into the background). This again shows that the majority of the variation occurs in the partial desorption regime and also gives an idea as to the range of chemical concentration variation in the gradient line.

The general trend in the oxygen concentration variation, observed in the experiments, can also be understood theoretically by considering the functional behavior of the governing equation for thermally driven desorption of SAM. The desorption profile
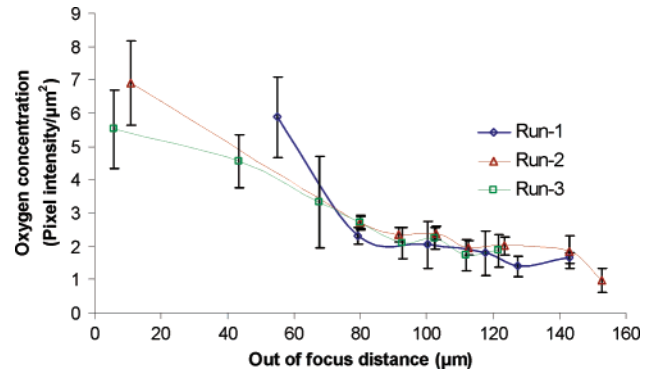
of points along the gradient, the beam radius becomes a variable (diverging beam as a substrate is moved out-of-focus). Hence, the temperature induced at various points along the scan varies inversely to the radius of the laser beam. It should be noted that the previous approach resulted in treating a dynamic process with a quasi-static solution of equations; as such, it is more appropriate to use the findings to predict the trend rather than relying on absolute values.

Including the relation between temperature induced and radius of beam in the thermokinetic model's functional dependence (eq 2), it can be seen that the fraction of HDT desorbed (ψ) varies in the following functional form:

$$\psi(r) \propto \left(1 - \exp\!\left(\frac{-1}{r}\right)\right) \qquad (4)$$

where $\psi(r)$ is the amount of HDT desorbed as a function of r. The functional relationship between the out-of-focus distance (z) and the radius of the beam (r), according to the theory of divergence of a laser beam, is given by eq 5[22]

$$r(z) = r_0\left[1 + \left(\frac{\lambda z}{\pi r_0^{\,2}}\right)^2\right]^{1/2} \qquad (5)$$

where $r(z)$ —is the 2e-folding radius of the diverged laser beam, r_0 —is the 2e-folding focal beam spot radius, and λ —is the wavelength of the laser. Combining eqs 4 and 5, the desorption as a function of out-of-focus distance, $z\,(\psi(z))$, is given by eq 6 and is plotted in Figure 12 to be compared with the experimental data

$$\psi(z)\alpha\left(1 - \exp\!\left(\frac{-1}{r_0\left[1 + \left(\frac{\lambda z}{\pi r_0^{\,2}}\right)^2\right]^{1/2}}\right)\right) \qquad (6)$$

The variation in oxygen concentration signifying the second SAM molecule concentration is proportional to the amount of primary SAM desorbed. The theoretical trend for desorption (at a point) along the gradient line, as a function of the out-of-focus distance, can be compared to the experimental data obtained for average oxygen intensity (calculated from the fitted curves for the oxygen signal from SIMS) variations. Given the uncertainties in the data points, it can be seen that the theoretical trend describes a variation in oxygen concentration as a function of the out-of-focus distance.
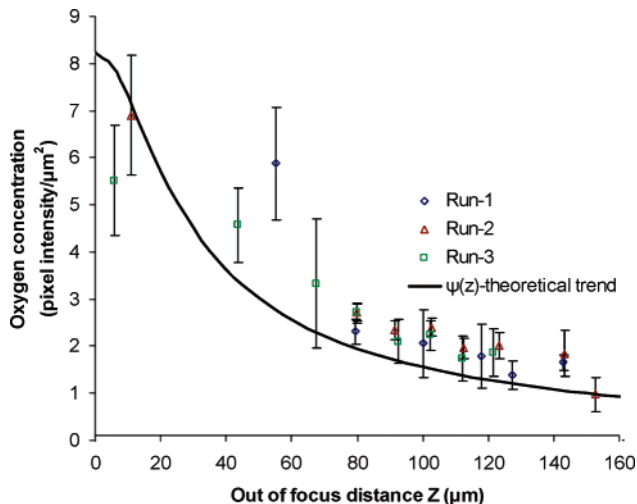

Figure 12. Theoretical trend for desorption as a function of out-of-focus distance, based on the thermokinetic model. It can be seen that the theoretical trend follows experimental data, given the associated uncertainties.

4. Conclusion

A new methodology to fabricate surface energy gradients on SAMs using DLP was developed. The method was demonstrated by fabricating a wettability gradient using HDT and MHA as contrasting SAMs. It is a simple, noncontact method and can also be easily extended to other systems such as chlorosilanes. Furthermore, there is no need for photolithography, either directly or indirectly.

Condensation imaging qualitatively showed the gradients produced. Using quantitative methods of SIMS, the desorption of HDT was found to be the most sensitive for incident laser intensity ranging between 29.15 and 6.5 kW/cm^2. The threshold laser intensity for desorption of HDT using the $10\times$ Olympus objective was found to be 1.9 kW/cm^2. The theoretical trend for the desorption, as a function of out-of-focus distance, was determined by considering the functional behavior of the governing equations. In general, it was found that the theoretical trend for desorption, as a function of out-of-focus distance, represented the experimental data.